

Cite this: DOI: 10.1039/xxxxxxxxxx

Cooee bitumen: Dynamics and structure of bitumen-water mixtures

Claire A. Lemarchand,^{*a} Michael L. Greenfield,^b and Jesper S. Hansen^a

Received Date
Accepted Date

DOI: 10.1039/xxxxxxxxxx

www.rsc.org/journalname

Systems of Cooee bitumen and water up to 4 mass % are studied by molecular dynamics simulations. The cohesive energy density of the system is shown to decrease with an increasing water content. This decrease is due mainly to an increase in potential energy which is not high enough to counterbalance the increase in volume due to the addition of water. It is not due to a decrease of potential energy between the slightly polar asphaltene molecules. The water molecules tend to form a droplet in bitumen. The size and the distribution of sizes of the droplets are quantified, with multiple droplets being more stable at the highest temperature simulated. The droplet is mainly located close to the saturates molecules in Cooee bitumen. Finally, it is shown that the water dynamics is much slower in bitumen than in pure water because it is governed by the diffusion of the droplet and not of the single molecules.

1 Introduction

Water is one of the main causes for pavement deterioration.¹⁻³ The mechanism by which water causes pavement failure is complicated and multiple: water may create a loss of adhesion between the bitumen binder and the aggregates, and/or a loss of cohesion inside the bitumen, and/or the bitumen-filler mastic.¹⁻³ On the other hand, water can be used beneficially in the context of road pavements. Bitumen emulsions, which are formed by injecting a few percent of water into hot bitumen are used to pave roads at much moderate temperatures, between 13°C and 23°C.⁴ The emulsion has a much lower viscosity than the bitumen itself allowing for an easier mixing with the aggregates.⁴ After the mixing step, the water evaporates over several months leaving bitumen with 0 to 4% in mass of water in its driest state.⁴

One of the reasons why the role of water in bitumen is so complex and rich is that bitumen is very hydrophobic,^{5,6} while some of the large aromatic molecules in bitumen, known as asphaltene molecules, are slightly polar. They are believed to stabilize the water-in-oil emulsion⁷ and even assemble more closely in the presence of water.⁸ This complex interplay between water and bitumen explains why the mechanism by which water causes pavement deterioration is still debated. In this context, the aim of this article is to address two main questions: (i) How is the structure

and internal cohesion of bitumen changed in the presence of water? (ii) How and how fast do the water molecules travel inside the bitumen?

To answer these two questions, we use molecular dynamics (MD) simulations of a modified model bitumen, known as Cooee bitumen.⁹ This model bitumen contains four molecule types chosen to resemble the Hubbard-Stanfield classification.¹⁰ The asphaltene and resin molecules of this model contain 2 and 1 sulfur atoms, respectively. The sulfur atom is chosen because it is by far the most common heteroatom in most bitumens.¹¹ The polarity due to the presence of this heteroatom is taken into account in the MD simulations by adding a partial charge on the sulfur atom and on the neighboring carbon atoms. Several systems with a growing concentration of water molecules are considered. For each of them, the cohesion and structure of bitumen are quantified using the cohesive energy of each molecule type, the radial distribution function and the average size of the nanoaggregates in bitumen. The structure and dynamics of the water molecules are quantified using the Delaunay tessellation, mean squared displacement and hydrogen bond dynamics.

The paper is organized as follows. Section 2 contains the necessary information about the molecular model and the simulations. In Sec. 3, results on the bitumen cohesive energy and structure as well as on the structure and dynamics of water are discussed. Section 4 contains a summary and a conclusion.

2 Molecular model and simulation details

The molecular model is the Cooee bitumen model⁹ which consists of four constituent molecule types, representing the asphalt-

^a DNRF Centre "Glass and Time", IMFUFA, Department of Sciences, Roskilde University, Universitetsvej 1, Postbox 260, DK-4000 Roskilde, Denmark. E-mail: clemarch@rip.ens-cachan.fr

^b Department of Chemical Engineering, University of Rhode Island, Kingston, Rhode Island USA 02881

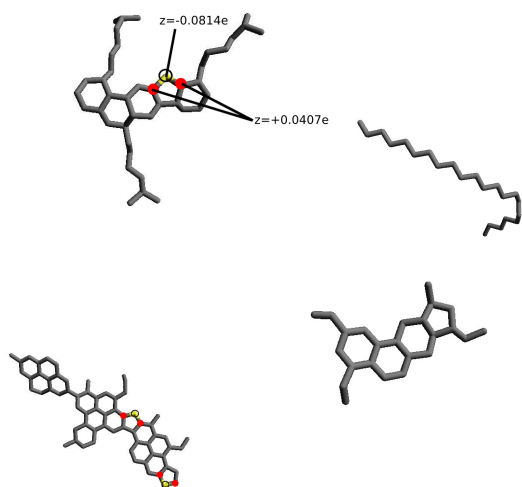


Fig. 1 (Color online). Constituent molecules in the Cooe bitumen model. Top left: Resin. Top right: Docosane (saturated hydrocarbon). Lower left: Asphaltene. Lower right: Resinous oil. Yellow indicates sulfur atoms having partial charge $z = 0.0814e$, and red circles indicate methylene group with partial charge $z = 0.0407e$, these are labeled C_2 . Hydrocarbon groups with zero charge are labelled C_1 . e is the fundamental unit of charge $e = 1.602 \times 10^{-19}$ C.

tene, resin, resinous oil and hydrocarbon components in bitumen. The structures of the four molecules chosen are presented in Fig. 1. This classification is based on the Hubbard-Stanfield scheme.^{10,12} In the original model, methyl, methylene, and methine groups are represented by the same Lennard-Jones particle, *i.e.*, a united atomic unit (UAU). The sulfur atom is also a Lennard-Jones particle, but with a different mass. In the presence of water, electrostatic interactions may be important, and in this work we include these into the Cooe model using a simple point charge model. In this way, the two methylene groups forming bonds with a sulfur are labeled C_2 and are each given a partial positive charge of $z = 0.0407e$ ¹³ as this group is less electronegative than sulfur. Likewise the sulfur is given a partial negative charge of $z = -0.0817e$, ensuring charge neutrality. Carbon-based groups not forming bonds with sulfur are labeled C_1 and have zero charge.

The force field is a simple extension of the original Cooe bitumen force field:

$$U(\mathbf{r}) = \sum_i \sum_{j>i} 4\epsilon_{ij} \left[\left(\frac{\sigma_{ij}}{r_{ij}} \right)^{12} - \left(\frac{\sigma_{ij}}{r_{ij}} \right)^6 \right] + \sum_i \sum_{j>i} \frac{z_i z_j}{4\pi\epsilon_0 r_{ij}} + \frac{1}{2} \sum_{\text{bonds}} k_s (r_{ij} - l_b)^2 + \frac{1}{2} \sum_{\text{angles}} k_\theta (\cos \theta - \cos \theta_0)^2 + \sum_{\text{dihedrals}} \sum_{n=0}^5 c_n \cos^n \phi. \quad (1)$$

The first two sums deal with pair interactions and the last three with the intramolecular interactions. Parameters for the intramolecular interactions in bitumen are given in Ref.⁹ The pair-interaction parameters are listed in Table 1 in SI units. The simulations are performed in reduced units such that $\sigma_{C_1 C_1} = 1$, $\epsilon_{C_1 C_1} = 1$, $m_{C_1} = 1$, $k_B = 1$ and $4\pi\epsilon_0 = 1$. The parameters between

particles with different Lennard-Jones interactions are given by the Lorentz-Berthelot mixing rules.¹⁴ To reduce the computational time, we approximate the electrostatic force calculations by a shifted force method, *i.e.*, the force is

$$F_c = \frac{z_i z_j}{4\pi\epsilon_0} \left(\frac{1}{r_{ij}^2} - \frac{1}{r_c^2} \right) \text{ if } r_{ij} \leq r_c, \quad (2)$$

using a cutoff of $r_c = 16.9 \text{ \AA}$. For non-confined systems the shifted-force approximation performs surprisingly well^{15,16} and is applicable here.

The water model is based on the SPC/Fw model^{17,18} which is a flexible three-site model. The force field is given by Eq. (1), with intramolecular parameters $k_s/k_B = 268089 \text{ K \AA}^{-2}$, $k_\theta/k_B = 38152 \text{ K rad}^{-2}$, $l_b = 1.012 \text{ \AA}$, and $\theta_0 = 1.91 \text{ rad}$. Due to computational efficiency, the values of these parameters are modified compared to Refs.^{18,19} such that the equilibrium angle value θ_0 is closer to the experimental value and the bonds are less rigid. The pair interaction parameters are listed in Table 1.

Table 1 Pair interaction parameters for the bitumen and water system. Parameters between particles with different Lennard-Jones interactions are given by the Lorentz-Berthelot mixing rules

X	σ_{XX} (\AA)	ϵ_{XX}/k_B (K)	m (g/mol)	z (e)
C_1	3.75	75.4	13.3	0
C_2	3.75	75.4	13.3	0.0407
S	3.75	75.4	32.0	-0.0814
O	3.15	78.4	16.0	0.82
H	-	0.0	1.0	-0.41

In all simulations we use 30 resin, 30 resinous oil, 30 asphaltene and 246 docosane molecules. Different systems with varying water contents are investigated, namely, with $n_W = 0, 5, 10, 20, 40, 70, 100, 150, 200$ and 300 water molecules. It corresponds to a mass fraction of water varying from 0 to 4%. The mass density is chosen so that the average pressure is equal to 1 atm. Three temperatures are investigated in detail, namely, $T = 603.2 \text{ K}$, $T = 452.4 \text{ K}$, and $T = 377.0 \text{ K}$ (reduced temperatures $T^* = k_B T / \epsilon_{C_1 C_1} = 8.0, 6.0, 5.0$). For these three temperatures and for all systems, eight independent initial configurations are considered. The equilibration time for each simulation is of 50 million steps followed by a production run of 50 million time steps also. It corresponds to 43 ns. Moreover, for all systems, one simulation run is performed for temperatures ranging from $T = 603.2 \text{ K}$ to $T = 301.6 \text{ K}$ by steps of 37.7 K. It enables us to see the effect of temperature with more accuracy. For these simulations the equilibration period is 40 million time steps and the production period 20 million time steps. These extensive runs are performed on a GeForce GTX 780 Ti graphics card using the RUMD software package²⁰ version 3.0.

The sizes of water droplets were determined using a geometric analysis.²¹ The simulation box was subdivided into tetrahedra using Delaunay tessellation. Atoms are located at each vertex, and the Delaunay algorithm²² ensures that no atoms are located within a tetrahedron. Droplets were defined by (1) identifying tetrahedra with at least two vertices being oxygen or hydrogen atoms of a water molecule, (2) noting which of these tetrahedra

shared common faces, and (3) iteratively grouping together such tetrahedra with the neighbors of their neighboring tetrahedra until all regions that share connectivity were connected. These are called “clusters” in the language of Ref.²¹ Periodic boundary conditions were accounted for when defining each tetrahedron. Restricting the tetrahedra to those with 3 or 4 atoms being from water leads to similar results as those shown below.

The volume of a droplet reported here equals the sum of the volumes of tetrahedra in a cluster. The water molecules within a droplet correspond to the water molecules that define the tetrahedra in a cluster. The number of droplets was determined by choosing a minimum cluster volume of 1 \AA^3 .

Geometry calculations were performed on configurations taken each $2^{20} = 1.05 \times 10^6$ time steps (48 per production run) for 4 of the 8 independent runs. Results were averaged separately for each combination of droplets, i.e. separate averages and distributions were calculated for drops 1 to n (in decreasing volume) when n droplets happened to be present. These results were combined to create averages over the largest droplet in each configuration.

3 Results and discussion

3.1 Bitumen cohesion and structure

The presence of water is believed to reduce the cohesion inside bitumen.^{1–3} The MD simulations allow us to check this hypothesis and also to study more precisely which molecule types are the most affected in their internal cohesion and structure in the presence of water.

Following the usual definition of the cohesive energy density²³ as the internal energy of vaporization of the liquid over the volume of liquid, we defined the cohesive energy density of the water-bitumen mixture in the following way:

$$ced = -\frac{U^{\text{tot}} - U^{\text{intra}}}{V}, \quad (3)$$

where U^{tot} is the total potential energy in the system, U^{intra} the intramolecular potential energy between UAUs in the same molecule, and V the volume of the system. The term U^{intra} includes intramolecular bonding and non-bonding interactions; adding the kinetic energy would lead to the internal energy of the set of molecules as an ideal gas. Figure 2 (a) shows the variation of the cohesive energy density ced with the number of water molecules in the system for three different temperatures. The values of the cohesive energy in the absence of water found in the simulations are in agreement with experimental results on the Hildebrand solubility parameter $\delta = \sqrt{ced}$ of bitumen. Ref.²⁴ reports Hildebrand solubility parameters of bitumen between $15.3 \text{ (MJ/m}^3)^{1/2}$ and $23 \text{ (MJ/m}^3)^{1/2}$, which corresponds to a cohesive energy between 2.3 and $5.3 \times 10^8 \text{ Pa}$. The simulation results lie exactly in this range. Likewise, the decrease of the cohesive energy density with temperature is very common.²⁵ Figure 2 (a) shows clearly that, in the simulations, the cohesive energy density decreases with the water content. This is so at all temperatures, although the trend is more visible as the temperature increases.

This result can be investigated further. In particular, the contri-

butions to the cohesive energy of the different molecule types in each system can be quantified for different water contents. The cohesive energy for a molecule of type X is defined as

$$ce_X = -\frac{(U_X^{\text{tot}} - U_X^{\text{intra}}) \mathcal{N}_A}{N_X}, \quad (4)$$

where N_X is the total number of molecules of type X in the system, \mathcal{N}_A the Avogadro constant, U_X^{tot} the total potential energy between the molecules of type X in the system, and U_X^{intra} the intramolecular potential energy of the molecules of type X in the system. Thus, the difference between these two energies corresponds to the intermolecular energy between the molecules of type X only. The molecule type can be Ar for aromatic, D for docosane (the saturates in the Coocoe model), or W for water. In the total cohesive energy density ced , the cross terms, corresponding to the intermolecular energy between different molecule types, also matter. They are defined here as:

$$ce_{X-Y} = -\frac{U_{X-Y}^{\text{inter}} \mathcal{N}_A}{(N_X + N_Y)}, \quad (5)$$

where U_{X-Y}^{inter} is the intermolecular energy between molecules of type X and Y . With these definitions, the total cohesive energy density ced can be expressed as:

$$ced = \frac{1}{V} \left(\sum_X \frac{N_X}{\mathcal{N}_A} ce_X + \sum_{X \neq Y} \frac{N_X + N_Y}{\mathcal{N}_A} ce_{X-Y} \right), \quad (6)$$

where the sum $\sum_{X \neq Y}$ is done over all distinct pairs (X, Y) such that $X \neq Y$. Figure 2 (b) shows the variation of the different contributions ce_X and ce_{X-Y} with the water content at $T = 377 \text{ K}$. The contributions involving water molecules, namely ce_{D-W} and ce_{Ar-W} , are growing with an increasing water content, while ce_W increases slightly. It means that the energetic contribution $N_W ce_W$ grows faster than linearly with an increasing water content. This is not so surprising as the addition of one water molecule when only a few water molecules are present causes the whole hydrogen bonded network to reorganise. The other contributions to the cohesive energy stay constant. Consequently, the overall decrease of the cohesive energy density ced is not due to a decrease of the cohesive energy inside bitumen, but rather to an increase in volume. In other words, when water molecules are added, the volume of the system increases, some contributions to the cohesive energy increase, but if bitumen molecules were added instead to match the same volume, the cohesive energy would increase more. In total, the cohesive energy density decreases. When the temperature increases, the picture is slightly different. Figures 2 (c) and (d) show the variation of the two cohesive energies ce_{Ar} and ce_D , respectively, with the number of water molecules in the system, for three different temperatures. The cohesive energy ce_{Ar} associated to aromatic molecules stays constant with the water content at all temperatures. However, the cohesive energy ce_D associated to docosane molecules decreases with the water content at high temperatures. Thus, at high temperatures, the overall decrease of the cohesive energy density ced is due both to an increase in volume and to a decrease of the cohesive en-

ergy in the docosane part of bitumen. The distinction between docosane and aromatic molecules at high temperatures regarding their intrinsic cohesive energy when water is added can be surprising. Indeed, the aromatic molecules contain the slightly polar asphaltene and resin molecules, which are usually believed to interact more with water^{7,8} than with the apolar saturates. If it was so, the water molecules should be located mainly close to the aromatic molecules, replacing interactions among aromatic molecules by interactions between water and aromatic molecules and thus decreasing the intrinsic cohesive energy of the aromatic molecules. This is not observed. Instead, it is the intrinsic cohesive energy of the docosane molecules which is lowered, suggesting that water molecules are mainly close to docosane molecules and not to aromatic molecules.

The idea that water molecules are closer to the saturates than to the polar aromatics can be directly checked using radial distribution functions. The radial distribution functions between the oxygen atom of the water molecules and the atoms in other molecules types are displayed for the system with $n_w = 5$ water molecules and at temperature $T = 377$ K in Fig. 3. This figure shows that the atoms closest to oxygen atoms, except hydrogen atoms from other water molecules, are from docosane molecules. This result stays true for other temperatures and other water contents in Cooe bitumen. We believe that water molecules are closer to docosane molecules than to aromatic molecules because aromatic molecules are part of the nanoaggregates. Nanoaggregates are composed of aligned flat aromatic molecules in the simulations. They are also a supramolecular structure identified experimentally in bitumen.²⁶ The nanoaggregates are held together in the Cooe model by Lennard-Jones interactions between many aligned united atoms. This can be seen as a model of the π -stacking interaction existing between aromatic molecules in real bitumen. The electrostatic interaction between the positively charged hydrogen of a water molecule and the slightly negatively charged sulfur atom of an asphaltene or resin molecule is negligible compared to the interaction holding the nanoaggregates together. Thus, water molecules are unlikely to penetrate the nanoaggregates and have no other choice than to stay close to the docosane molecules. We would like to stress here that this result could be altered if the polarity of the asphaltene and resin molecules is increased enough, or if they have the possibility to form hydrogen bonds. However, the molecular structures used in this work for asphaltene and resin molecules are believed to be representative.

The variation of the intrinsic energy of the aromatic molecules ce_{Ar} with temperature and water content deserves some further discussion. As already mentioned, the aromatic molecules in the Cooe bitumen are known to align in nanoaggregates. The definition of the nanoaggregates in the case of Cooe bitumen is detailed in Refs.^{27,28} It sums up to the following rule: two aromatic molecules are nearest neighbors in the same nanoaggregate if they are well aligned and close enough. More specifically, this rule is based on three thresholds. The first threshold quantifies how much the molecules should be aligned to be declared in the same nanoaggregate. This first threshold imposes boundaries to the angle θ between the normal vectors to the aromatic

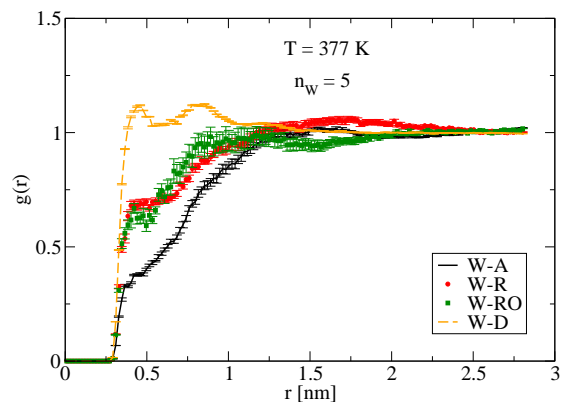


Fig. 3 Radial distribution function between oxygen atoms in water molecules and other atoms in other types of molecules for $n_w = 5$ at temperature $T = 377$ K. Error bars correspond to standard deviation on the data divided by the square root of the number of independent initial configurations considered.

planes of two different molecules. We choose $0^\circ \leq \theta \leq 34^\circ$ and $149^\circ \leq \theta \leq 180^\circ$.²⁷ The second threshold is related to how close the molecules should be to be declared in the same nanoaggregate. This second threshold imposes a maximum value to the distance d_1 between the aromatic planes of two different molecules. We impose $d_1 \leq 6 \text{ \AA}$.²⁷ Two molecules far away but in the same plane can have a very low distance d_1 . This is why a third threshold is needed. The third threshold imposes a maximum value to the distance d_2 between the center of mass of the first molecule and the projection of the center of mass of the second molecule on the plane of the first molecule. We fix $d_2 \leq 0.7d_A \text{ \AA}$,²⁷ where $d_A = 13.1 \text{ \AA}$ is the typical length of an asphaltene molecule in the Cooe model. Some nanoaggregates are branched, because the asphaltene molecule chosen in the Cooe model has a flat head and a flat body oriented in different directions, and both parts can align with other aromatic molecules. The average number of aromatic molecules inside a nanoaggregate is used to quantify the size of the nanoaggregates. The variation of the nanoaggregate size with the water content is displayed in Fig. 4 for three different temperatures. This figure shows that within error bars and for all temperatures, the nanoaggregate size does not depend on the water content. This is in agreement with the intrinsic cohesive energy of the aromatic molecules being independent of the water content. Surprisingly, the variation of the nanoaggregate size with temperature is non-monotonic. This fact has been reported and explained.²⁸ It is due to two competing effects when temperature increases: the first effect is the increase of thermal noise which tends to detach molecules from the nanoaggregates and decrease the nanoaggregate size; the second effect is the relative increase of the number of asphaltene molecules inside the nanoaggregates compared to other molecule types, which tends to increase the degree of branching of the aggregates and also their size. The non-monotonic behavior of the cohesive energy ce_{Ar} between aromatic molecules is due to the same cause.

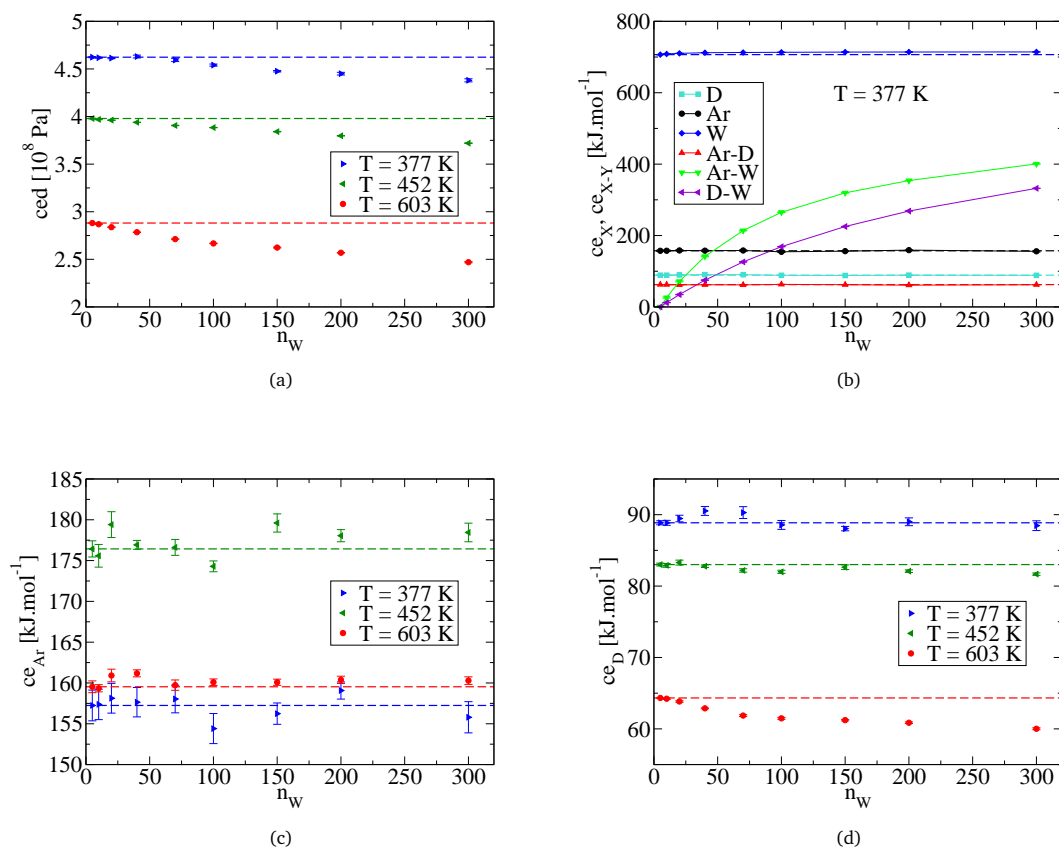


Fig. 2 (a): Variation of the cohesive energy density ced with the number of water molecules n_W for different temperatures. (b): Variation of each contribution to the cohesive energy density as described in Eq. 6 with the number of water molecules for $T = 377$ K. The dashed horizontal lines correspond to the value at $n_W = 5$. (c) and (d): Variation of the cohesive energy between aromatic molecules ce_{Ar} and docosane molecules ce_D , respectively, with the number of water molecules n_W for different temperatures.

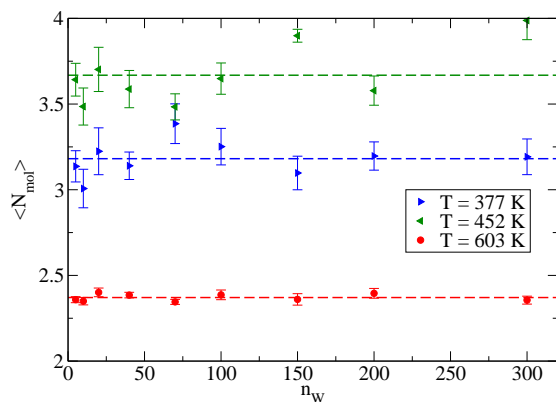


Fig. 4 Variation of the average number of aromatic molecules $\langle N_{\text{mol}} \rangle$ with the number of water molecules n_W for different temperatures. The dashed horizontal lines correspond to the average value over all values of n_W for the same temperatures.

Finally, the variation of the bitumen dynamics with the water content can be checked. Figure 5 displays the time evolution of the mean squared displacement of the centers of mass of the asphaltene molecules for different water contents and at temperature $T = 377$ K. The shape of the curves is characteristic of that of a viscous liquid. At short time scales a ballistic regime is visible. It is followed by a plateau at intermediate times and finally a diffusive regime is recovered. All curves collapse, which shows that the asphaltene dynamics do not depend on the water content. The same result is found for the dynamics of the saturates molecules (not shown).

3.2 Water droplet

The water molecules present in bitumen generally form a droplet, as can be seen in Fig. 6 for one configuration of the system with $n_W = 300$ water molecules and at temperature $T = 452$ K. The water distribution among droplets and the droplet sizes were quantified by Delaunay tetrahedra for which at least 2 of 4 vertex atoms belonged to a water molecule.

The droplet volume was approximated as the volume of adjoining tetrahedra that form a cluster. The distribution of droplet volumes under all conditions are shown in Fig. 7. The y-axis indicates the probability that a volume V of water can be found within droplets of volume between V and $V + dV/V$; it is normalized so $\int P(V)d \ln V = 1$. Results at 377 K show that a range of droplet sizes can occur. While most volume is usually found in a single large droplet, significant numbers of cases were found with multiple droplets with volumes between 90 and 200 \AA^3 for the $n_W = 300$ system. Similar results were found for $n_W = 200$ to 70 water molecules. Only a single large droplet was typical for systems with fewer than 70 water molecules.

Results at 452 K differ in that only a single droplet size was prevalent at each composition. This potentially reflects better equilibration of the bitumen–water phase behavior due to faster water diffusion over nanosecond time scales (see below).

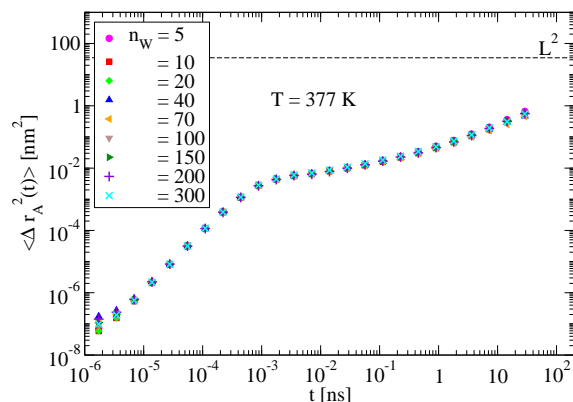


Fig. 5 Time evolution of the mean-squared displacement of the center of mass of the asphaltene molecules for different numbers of water molecules n_W at temperature $T = 377$ K. The dashed black line indicates the value of the box length squared (L^2), in the case of $n_W = 5$.

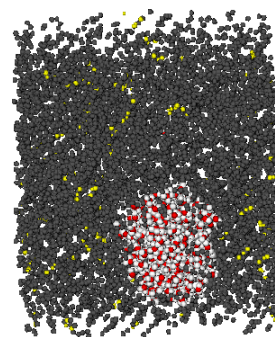


Fig. 6 (Color online) Snapshot of the $n_W = 300$ system at $T = 452$ K. All carbon-based UAU are grey, sulfur atoms are yellow, hydrogen white and oxygen red.

Results at 603 K show a qualitative difference. A broad distribution of drop sizes over a 1 to 70 \AA^3 range is present at all water compositions. For $n_w \leq 40$, most volume is found within states of $V < 1 \text{\AA}^3$. These correspond to individual water molecules. Coalescence into larger droplets occurred for $n_w = 100$ and larger, though more water molecules remained outside the largest droplet than in the 377 and 452 K cases.

Two measures of the droplet volume are shown in Fig. 8. Solid lines indicate the total volume of Delaunay tetrahedra that constitute large water droplets ($V \geq 1 \text{\AA}^3$). Dashed lines indicate the volume of only the largest droplet. Error bars indicate standard deviations on the size of the largest droplet present, averaged over all configurations considered.

The total droplet volume increases approximately linearly with the number of water molecules in the system. Deviations from linearity are most notable at the highest temperature for the smaller numbers of water molecules, i.e. the cases that are dominated by an absence of coalesced droplets. Linearity indicates a homogeneous water environment as the number of water molecules increases.

The average volumes of only the largest droplets indicate differences among the three temperatures that are consistent with the volume distributions. Many drops are present in the 603 K case, leading to the largest drop containing only a small to moderate fraction of the total drop volume until a large number of water molecules are present (mass fraction of ca. 1.6%). Some cases of multiple droplets at 377 K lead to similar but much smaller effects at that temperature at larger numbers of water molecules. The larger error bars at high n_w for both temperatures are a consequence of the volume differences for the largest droplet when 2 or more droplets are present, such as 220\AA^3 vs. 180\AA^3 in the case of 1 or 2 droplets at 377 K with $n_w = 300$ (see Fig. 7). Results at 452 K show a more predominant occurrence of a single large droplet. Cases of multiple large droplets were sufficiently rare at this temperature to lead to negligible differences between the average volume of the largest droplet and of all large droplets.

The division of water molecules between large droplets and dispersed molecules was also determined from the geometric analysis. The number of water molecules that are not in droplets of $V > 1 \text{\AA}^3$ are shown in Fig. 9 by solid lines. It corresponds to the number of free water molecules. Error bars indicate standard deviations across all configurations. Essentially all water molecules are in droplets at 377 K, and the number of free water molecules increases with temperature. At 377 and 452 K, the number of free water molecules decreases as the total number of water molecules increases beyond $n_w = 10$ in the simulations. At 603 K, most water molecules are free for concentrations up to $n_w = 40$, then the number reaches a peak and decreases as the water concentration increases further. These results indicate that additional water molecules add to the largest droplet. This is consistent with a shift in the droplet size distribution to larger volumes, as seen in Fig. 7.

Dashed lines indicate the number of water molecules that are not in the largest droplet. Error bars indicate the standard deviation in the number of water molecules that are in the largest droplet; it applies to counting those not in the largest droplet be-

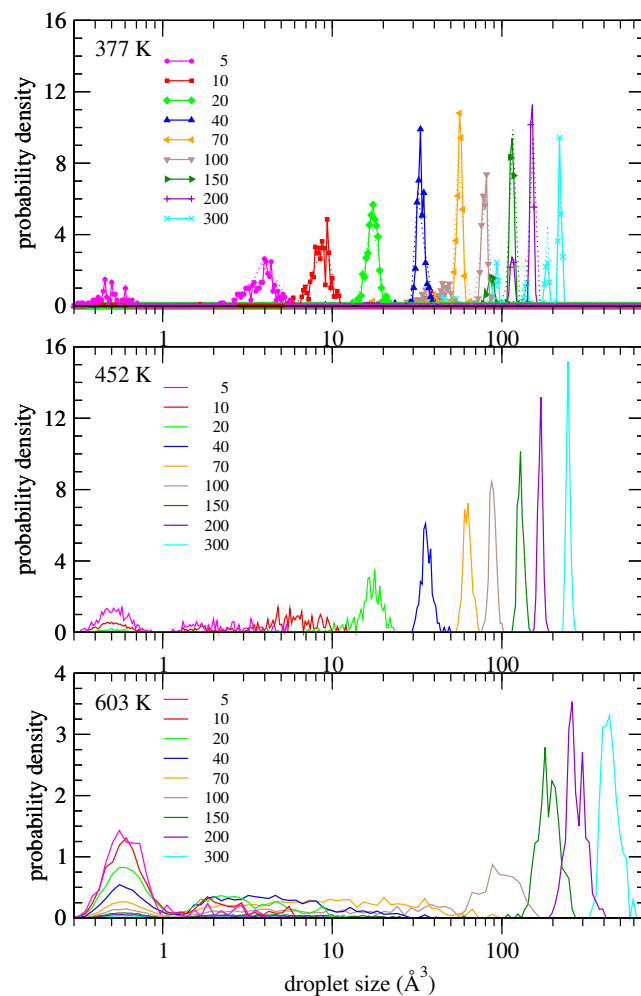


Fig. 7 (Color online) Volume-weighted distribution of droplet volumes at $T = 377, 452,$ and 603 K. Separate distributions are computed for each number of water molecules. Dotted lines indicate results at 377 K using only the final 1/3 of each trajectory.

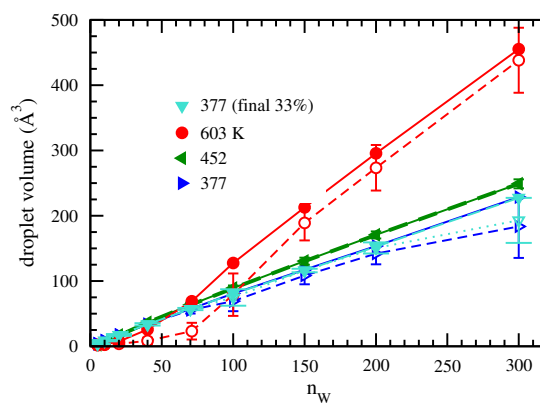


Fig. 8 (Color online) Average volume of the largest droplet (open symbols, dashed lines) and of all large droplets (closed symbols, solid lines) at temperatures 377, 452, and 603 K and at 377 K using the final 1/3 of the trajectory.

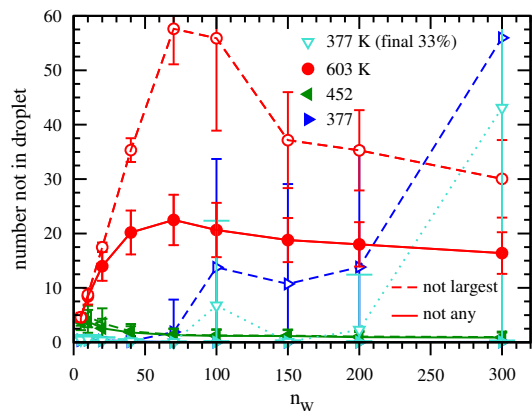


Fig. 9 (Color online) Number of water molecules not in the largest droplet (dashed line, open symbols) or not in any droplet (solid line, filled symbols) at temperatures 377, 452, and 603 K and at 377 K using the final 1/3 of the trajectory.

cause the number of molecules is constant in each simulation. Results at 603 K differ qualitatively by showing a large fraction of water molecules at all concentrations that are not in the largest droplet. This constitutes more than half of the water molecules for systems with up to 100 water molecules. Results at 452 K show essentially all water molecules belonging to a single large droplet.

Differences between 377 and 452 K are suggested by the results at higher numbers of water molecules. Multiple droplets exist at 377 K for $n_W = 100$ and larger when averaged over the entire simulation trajectory, which is consistent with the multiple peaks shown in Fig. 7. This leads to a significant number of water molecules outside of the largest droplet. However, further analysis shows that when multiple droplets exist in cases of $n_W = 40$ or more, they are present initially and coalesce into fewer droplets as the simulation proceeds. This suggests that a longer equilibration period would lead to one large droplet being predominant at 377 K, as is found at 452 K.

To test this idea, the 377 K results were reanalyzed by using only the final one third of the structures in each production run. Results are shown by dotted lines. The volume of the largest droplet (Fig. 8) shifts toward the volume of all large droplets as a consequence of droplets coalescing. Similarly, the number of water molecules not in the largest droplet decreases (Fig. 9). Changes in the size distributions (Fig. 7) are less apparent, in part because of the wide volume scale. A clear change is the loss of droplet volumes between 30 to 50 \AA^3 at $n_W = 100$. Droplets of this size coalesce with the main droplet and do not form again during the simulation. These results emphasize the long time scales required for structural relaxations at lower temperatures.

3.3 Water dynamics

The water dynamics are affected by the fact that water molecules tend to form a droplet. The water dynamics are first quantified using the mean squared displacement Δr_W^2 of the centers of mass of the single water molecules. This mean squared displacement is plotted versus time for different water contents and for tempera-

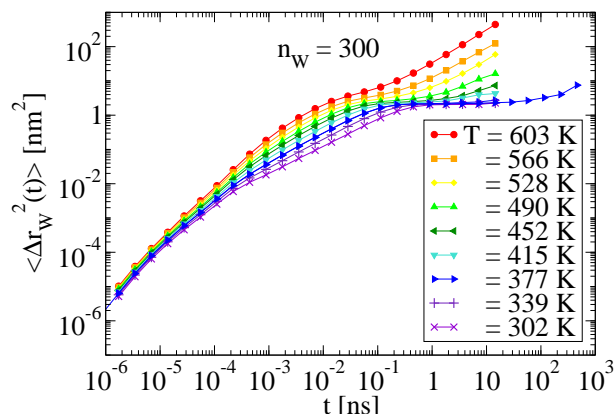


Fig. 11 Variation of the mean squared displacement $\Delta r_W^2(t)$ of the center of mass of water molecules with time for $n_W = 300$ at different temperatures.

ture $T = 377$ K and $T = 603$ K, in Figs. 10 (a) and (b), respectively. This figure also displays the mean squared displacement of pure water at the same temperature and pressure. The main result of this figure is that the water dynamics is slowed down significantly at long times in bitumen compared to its counterpart in pure water. This is true at all temperatures, although the slow down is larger at low temperatures. Surprisingly, the slow down is larger for large water contents than for low water contents. A diffusive regime is eventually reached at long times. The long-time diffusive regime is clearly visible at high temperatures and small water contents in Figs. 10 (a) and (b). It is also observable at the low temperature $T = 377$ K and for the largest water content $n_W = 300$, for a long enough simulation. This is shown in Fig. 11, displaying in particular the time evolution of the mean squared displacement of water molecules in a single simulation of 0.86 μs with $n_W = 300$ water molecules at $T = 377$ K. The diffusion constant of the long-time diffusion regime decreases with an increasing water content. This indicates that this regime corresponds to the diffusion of the water droplet inside the bitumen matrix. As the number of molecules increases, the droplet becomes heavier and its diffusion constant decreases. Of course, in the limit of many water molecules with a droplet of bitumen in it, the faster bulk water dynamics would be recovered, but this is not the limit studied in this work.

Two other interesting observations can be made on the time evolution of the mean squared displacement of water molecules at shorter time scales. The first observation is that the water dynamics in bitumen are slightly faster than the pure water dynamics at short times, between 10^{-4} and 10^{-3} ns, as can be seen in Figs. 10 (a) and (b). The smaller the number of water molecules, the faster the dynamics at these time scales. The second observation is that at intermediate times, around 10^{-2} ns, the water dynamics in bitumen becomes slower than in pure water, but the larger the number of molecules in bitumen, the closer to the bulk water dynamics. To interpret these observations, it is necessary to describe the time evolution of the mean squared displacement of

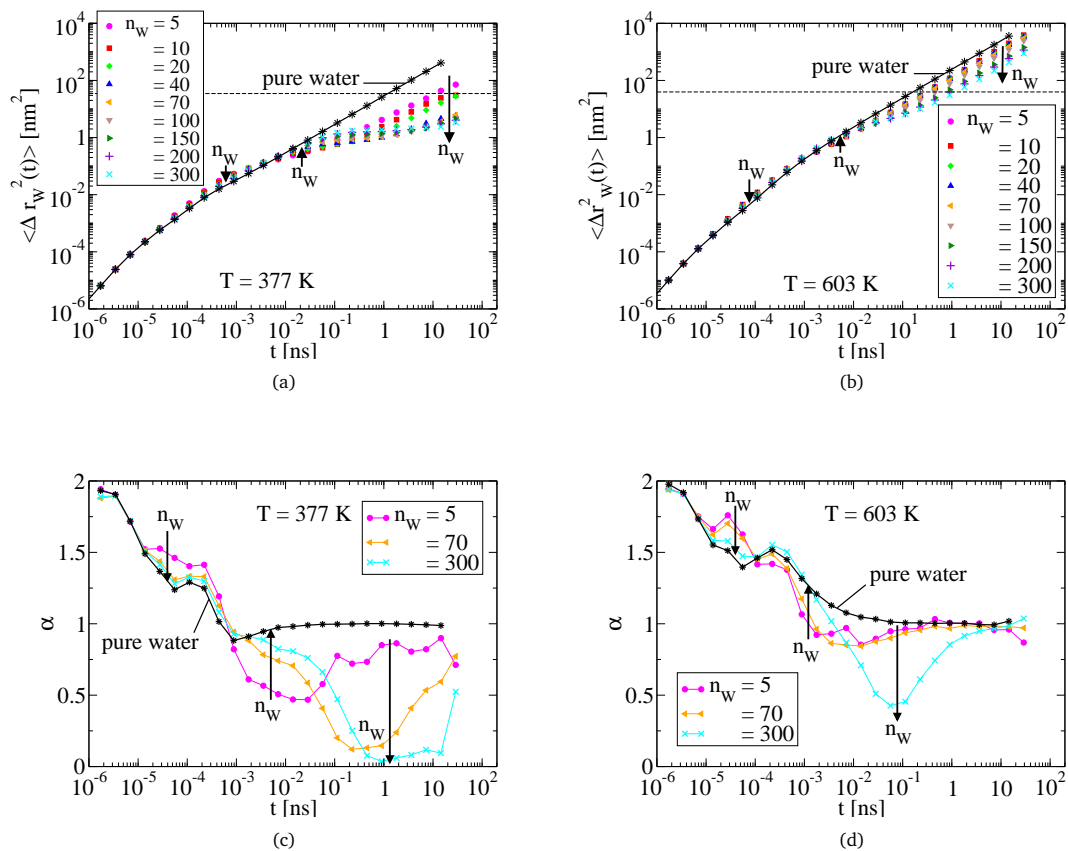


Fig. 10 Variation of the mean squared displacement $\Delta r_W^2(t)$ of the center of mass of water molecules with time for different number of water molecules and for temperatures $T = 377\text{ K}$ (a) and $T = 603\text{ K}$ (b). The black dashed line indicates the value of the box length squared, in the case of $n_W = 5$. (c) and (d): Variation of the exponent of the mean squared displacement curves in (a) and (b), respectively. For the sake of readability only curves corresponding to $n_W = 5, 70, 300$ are displayed.

water molecules more closely. An informative quantity in this respect is the local exponent $\alpha(t)$ of the mean squared displacement curve. It is defined as

$$\alpha(t) = \frac{\log \Delta r_W^2(t) - \log \Delta r_W^2(t - \Delta t)}{\log(t) - \log(t - \Delta t)}, \quad (7)$$

where Δt is increasing logarithmically in base 2. The time evolution of the local exponent α is displayed in Figs. 10 (c) and (d) for temperatures $T = 377$ K and $T = 603$ K, respectively. For the sake of clarity, the case of temperature $T = 377$ K is described in more details, results being qualitatively similar at other temperatures. In Fig. 10 (c), the ballistic motion is clearly visible at the beginning and corresponds to $\alpha = 2$. At time scales around 10^{-4} ns, the local exponent α is smaller than 2 and decreases more as the number of water molecules increases. In other words, when only a few water molecules are present in bitumen, it is as if the ballistic regime was maintained for longer times. This could be due to the fact that, as the number of water molecules decreases, water molecules interact with more bitumen molecules, with which the interaction is lower than with other water molecules, maintaining a ballistic motion for longer times. It explains why the water dynamics around 10^{-4} ns is slightly faster when the number of molecules in bitumen is lower, as seen in Fig. 10 (a). Around 10^{-3} ns, the regime becomes diffusive in bulk water, which is characterized by $\alpha = 1$. It corresponds to diffusion of water molecules in water. At this time scale, the regime becomes subdiffusive for water molecules in bitumen. The smaller the number of water molecules in bitumen, the earlier the start of the subdiffusive regime. For example, for $n_W = 5$ water molecules, the diffusive regime seen in bulk water is not reached and a subdiffusive regime settles in at 10^{-3} ns, whereas for $n_W = 300$ the diffusive regime of bulk water is followed up to 5×10^{-3} ns. This effect is likely due to water molecules feeling the edge of the water droplet. The bigger the droplet, the later this effect is observed. It explains why at a given time scale around 5×10^{-2} ns in Fig. 10 (a) the dynamics of water molecules is faster for a larger number of water molecules: they are not yet affected by the drop edge. At longer time scales and as already discussed, the water dynamics is governed by the diffusion of the water droplet inside bitumen. For large water contents, the final diffusive regime sets in after a long plateau, associated with a local exponent α close to zero, and corresponding to the water droplet being nearly arrested in bitumen.

To supplement the description of water dynamics in bitumen at short time scales, we looked at the hydrogen bond dynamics. Hydrogen bonds can be defined using an energetic or a geometric criterion in MD.^{29,30} We choose the geometrical definition described in Ref.,³¹ adapted to the water model used in this work. To be declared as bonded via a hydrogen bond, two water molecules should comply with the criteria:

1. The distance between the two oxygen atoms is less than $R_{OO} = 3.6 \text{ \AA}$.
2. The distance between the hydrogen atom of one molecule and the oxygen atom of the other is less than $R_{OH} = 2.45 \text{ \AA}$.

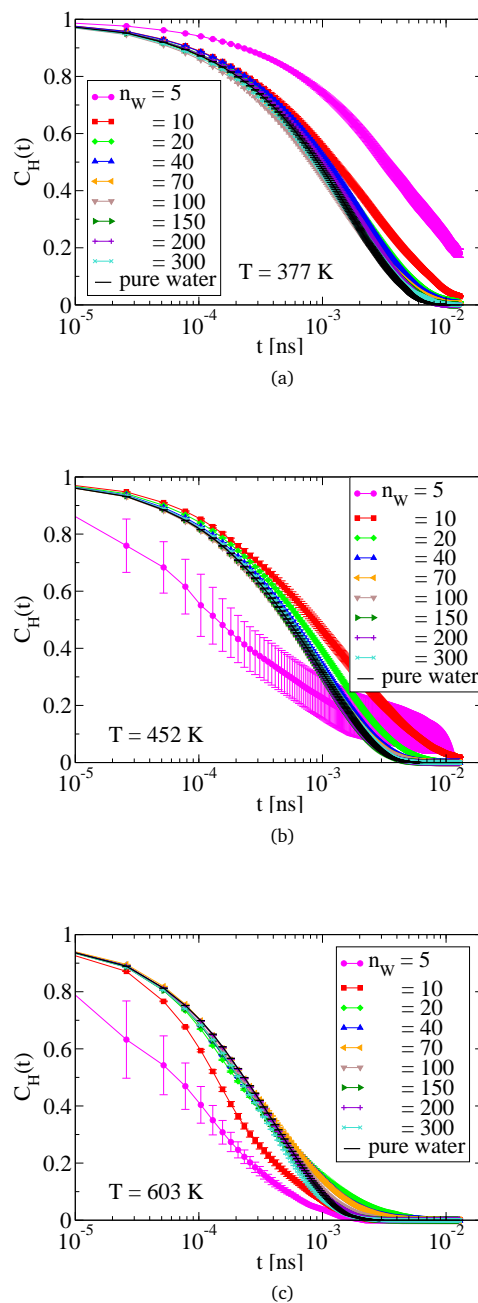


Fig. 12 Variation of the autocorrelation function $C_H(t)$ between hydrogen bonds with time for different number of water molecules and temperatures $T = 377$ K (a), $T = 452$ K (b), and $T = 603$ K (c).

3. The angle between the oxygen atom of one molecule, the oxygen atom, and the hydrogen of atom the other molecule is less than $\phi = 30^\circ$.

We used the following definition for the autocorrelation function $C_H(t)$ between hydrogen bonds:

$$C_H(t) = \frac{\langle h_{ij}(t_0, 0)h_{ij}(t_0, t) \rangle}{\langle h_{ij}(t_0, 0) \rangle}, \quad (8)$$

where $h_{ij}(t_0, t) = 1$ if the two water molecules i and j have been bonded without any breaking between time t_0 and time t and $h_{ij}(t_0, t) = 0$ otherwise. The average $\langle \cdot \rangle$ is done over all pairs (i, j) , with $i \neq j$, and over initial times t_0 . In this way, the correlation function is related to the lifetime of a single hydrogen bond.³¹ The time evolution of the correlation function $C_H(t)$ is plotted in Figs. 12 (a), (b), and (c) for different water contents and at temperature $T = 377$ K, $T = 452$ K, and $T = 603$ K, respectively. At temperature $T = 377$ K, the correlation functions associated to water molecules in bitumen tend to decay more slowly than the correlation function in bulk water. The more water molecules in bitumen, the closer to the correlation function of bulk water. It means that the droplet formed when the total number of water molecules n_W is low is stiffer than in bulk water. The same result is shown in another form in Fig. 13, displaying the variation of the half lifetime $\tau_{1/2}$ with the number of water molecules n_W at different temperatures. The half lifetime $\tau_{1/2}$ is defined as usual by $C_H(\tau_{1/2}) = 0.5$. Figure 13 shows that the lifetime of a hydrogen bond at the lowest temperature is around 1 ps, which is in agreement with other simulation³¹ and experimental³² results. At these time scales, according to Fig. 10 (a), the mean squared displacement of water molecules in the small stiff droplet is higher than that of bulk water. For a higher temperature $T = 452$ K a similar trend is observed: the higher the total number of water molecules n_W , the smaller the half lifetime $\tau_{1/2}$. At temperature $T = 603$ K, the inverse trend is observed. To explain this, one can note that the cases of a total number of water molecules $n_W = 5$ at $T = 452$ K and $T = 603$ K, and $n_W = 10$ at $T = 603$ K are singled out. The error bars on these results are quite large, because the initial number of water molecules linked by a hydrogen bond is low at these high temperatures and for such low numbers of water molecules. Indeed, Fig. 7 shows that the fraction of free water molecules in these 3 cases is very high. This leads to poor statistics on the correlation function and the overall results that these bonds do not last.

4 Summary and Conclusions

In a system containing Cooee bitumen and up to 4 % in mass of water, molecular dynamics simulations have shown several features that describe how water molecules self-organize. (i) There is a loss of cohesion in the bitumen when the water content is increased. But at temperature $T = 377$ K, this loss is due mainly to the fact that the interactions with water molecules do not increase enough to counteract the increase in volume. At very high temperatures, the overall loss of cohesion is also due to a loss of cohesion among the saturates molecules. The internal cohesion and structure of the aromatic molecules, assembled into nanoag-

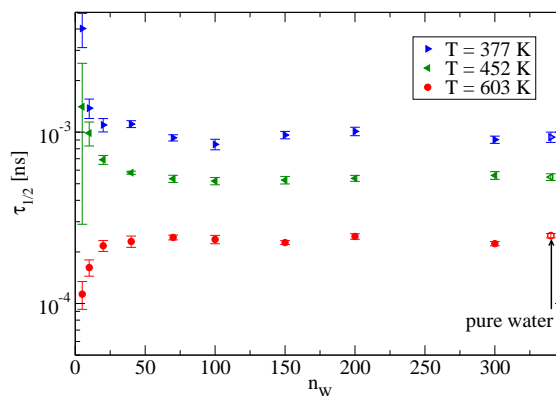


Fig. 13 Variation of the half lifetime of an hydrogen bond $\tau_{1/2}$ with the number of water molecules n_W for different temperatures. The open symbols correspond to the half lifetime in pure water at the same temperatures.

gregates, are unchanged as the water content increases.

(ii) The water molecules tend to form a droplet, which is mainly located next to saturates. Most water is in a single large droplet at 452 K, while some smaller droplets occurred initially at 377 K. A main droplet becomes dominant at 603 K only for the higher water concentrations studied. The number of water molecules outside the largest droplet reaches a plateau as the water concentration increases. The droplet volume increases linearly with the number of water molecules in the entire system.

(iii) The structure and dynamics of the water molecules are deeply affected by the presence of bitumen. At long times, the water molecules reach a diffusive behavior, but it is governed by the diffusion of the water droplet. The diffusion constant is consequently much lower than that of bulk water and decreases as the droplet mass increases. At short times, the hydrogen bond lifetime is higher in bitumen than in pure water at temperature $T = 377$ K and for a small number of water molecules. The droplet is stiff. When the number of water molecules increases, the hydrogen bond breaking of bulk water is recovered. On the contrary, at very high temperatures $T = 603$ K, the hydrogen bond dynamics is faster in bitumen containing a small number of water molecules than in bulk water. This is due to the fact that at these high temperatures, the water molecules need to be more numerous to form a hydrogen bonded network.

Two natural perspectives arise from the conclusions just drawn. The first one is to describe in more detail the dynamics of free water molecules. How long do they spend outside the main droplet? How far can they go? The second perspective is to study how the water structure and dynamics are affected in the presence of hydrophilic surfaces such as those of filler particles and aggregates. How many water molecules are left in bitumen in this case? How fast do the water molecules reach the hydrophilic surfaces.

References

- 1 G. D. Airey, A. C. Collop, S. E. Zoorob and R. C. Elliott, *Constr. Build. Mater.*, 2008, **22**, 2015–2024.
- 2 S. Cui, B. R. K. Blackman, A. J. Kinloch and A. C. Taylor, *Int. J. Adhes. Adhes.*, 2014, **54**, 100–111.
- 3 B. R. K. Blackman, S. Cui, A. J. Kinloch and A. C. Taylor, *Int. J. Adhes. Adhes.*, 2013, **42**, 1–10.
- 4 K. M. Muthen, *Foamed Asphalt Mixes - Mix Design Procedure*, External Contract Report CR-98/077, 1998.
- 5 M. Salou, B. Siffert and A. Jada, *Colloids Surf., A*, 1998, **142**, 9–16.
- 6 T. Kasongo, Z. Zhou, Z. Xu and J. Masliyah, *Can. J. Chem. Eng.*, 2000, **78**, 674–681.
- 7 O. C. Mullins, *Annu. Rev. Anal. Chem.*, 2011, **4**, 393–418.
- 8 M. R. Gray, R. R. Tykwinski, J. M. Stryker and X. Tan, *Energy & Fuels*, 2011, **25**, 3125–3134.
- 9 J. S. Hansen, C. A. Lemarchand, E. Nielsen and J. C. Dyre, *J. Chem. Phys.*, 2013, **138**, 094508.
- 10 R. Hubbard and K. Stanfield, *Anal. Chem.*, 1948, **20**, 460.
- 11 D. R. Jones IV, *Asphalt Cements: A Concise Data Compilation*, SHRP-A-645, Strategic Highway Research Program, 1993.
- 12 F. Rostler, *Asphalts, Vol. II*, John Wiley and Sons, 1965.
- 13 X. Liu, G. Zhou, X. Zhang and S. Zhang, *AIChE J.*, 2010, **56**, 2983.
- 14 M. P. Allen and D. J. Tildesley, *Computer Simulation of Liquids*, Oxford Science Publications, Oxford, 1987.
- 15 J. S. Hansen, T. B. S. der and J. C. Dyre, *J. Phys. Chem. B*, 2012, **116**, 5738–5743.
- 16 K. Takahashi, T. Narumi and K. Yasouko, *J. Chem. Phys.*, 2011, **134**, 174112.
- 17 K. Toukan and A. Rahman, *Phys. Rev. B*, 1985, **31**, 2643.
- 18 Y. Wu, H. J. Tepper and G. A. Voth, *J. Chem. Phys.*, 2006, **124**, 024503.
- 19 G. Raabe and R. J. Sadus, *J. Chem. Phys.*, 2007, **126**, 044701.
- 20 N. Bailey, T. Ingebrigtsen, J. Hansen, A. Veldhorst, L. Böhling, C. Lemarchand, A. Olsen, A. Bacher, H. Larsen, J. Dyre and T. Schröder, *submitted to J. Comput. Chem.*, 2015.
- 21 M. L. Greenfield and D. N. Theodorou, *Macromolecules*, 1993, **26**, 5461–5472.
- 22 M. Tanemura, T. Ogawa and N. Ogita, *J. Comput. Phys.*, 1983, **51**, 191–207.
- 23 M. R. J. Dack, *Chem. Soc. Rev.*, 1975, **4**, 211–229.
- 24 P. G. Redelius, *Fuel*, 2000, **79**, 27.
- 25 A. F. M. Barton, *Chem. Rev.*, 1974, **75**, 731.
- 26 O. C. Mullins, H. Sabbah, J. Eyssautier, A. E. Pomerantz, L. Barré, A. B. Andrews, Y. Ruiz-Morales, F. Mostowfi, R. McFarlane, L. Goual, R. Lepkowitz, T. Cooper, J. Orbulescu, R. M. Leblanc, J. Edwards and R. N. Zare, *Energy & Fuels*, 2012, **26**, 3986–4003.
- 27 C. A. Lemarchand, T. B. S. der, J. C. Dyre and J. S. Hansen, *J. Chem. Phys.*, 2013, **138**, 094508.
- 28 C. A. Lemarchand and J. S. Hansen, *accepted in J. Phys. Chem. B*, 2015.
- 29 A. Luzar and D. Chandler, *J. Chem. Phys.*, 1993, **98**, 8160.
- 30 J. A. Padro, J. Martí and E. Guàrdia, *J. Phys.: Condens. Matter*, 1994, **6**, 2283–2290.
- 31 J. Martí, J. A. Padro and E. Guàrdia, *J. Chem. Phys.*, 1996, **105**, 639.
- 32 S. Woutersen, U. Emmerichs, H.-K. Nienhuys and H. J. Bakker, *Phys. Rev. Lett.*, 1998, **81**, 1106.